Harmonic Phasor Estimator for P-Class Phasor Measurement Units

Lei Chen, Wei Zhao , Fuping Wang, and Songling Huang, *Senior Member, IEEE*

Abstract— Fast harmonic phasor measurements are very useful in power system protection applications, e.g., high-impedance fault location and intelligent method-based islanding detection. To address this problem, a novel harmonic phasor estimator is proposed in this paper, especially for P-class phasor measurement units (PMUs). The exponential functions are used to model the decaying dc (ddc) component, and the optimal time constant (TC) set for the ddc model is searched based on an enumeration method. In addition, the dynamic harmonic phasors are modeled based on the Shannon sampling theorem. As a result, a filter bank is designed for harmonic phasor and frequency estimations. The rate of change of frequency (ROCOF) of the harmonic is estimated based on a second-order fitting method. The response time of the proposed method for harmonic phasor estimation is always no longer than 40 ms. Simulation test results indicate that the proposed method is more accurate than the Taylor–Fourier transform (TFT) under ddc offset and frequency deviation conditions. In particular, the proposed method is more robust to ddc's TC variations. An experimental test is implemented to demonstrate the advantages of the proposed method.

Index Terms— Decaying dc (ddc) offset, exponential functions-based model, finite impulse response (FIR) filter, harmonic phasor, phasor measurement unit (PMU).

I. Introduction

NOWADAYS, harmonics are widely present in transmission and distribution networks. For example, high-impedance faults occurring in distribution networks can cause harmonics in current signals [1], [2]. Arcing faults in high/medium voltage transmission networks can also result in harmonic currents [3]. Distributed generations can also lead to harmonics because of the widely used nonlinear power electronic devices. Such harmonic information can be used in high-impedance fault identification/location [1], [2], arcing fault identification/location [3], and intelligent-based islanding detection [4]–[6]. Thus, it is necessary to develop a fast harmonic phasor estimator for these power system protection applications.

Recently, phasor measurement units (PMUs) are widely used in transmission networks for fundamental synchrophasor measurements. In the IEEE Standard C37.118.1-2011 and its amendment standard C37.118.1a-2014 (collectively called the

IEEE standard in the following) [7], [8], PMUs are divided into two classes, i.e., P class for protection applications and M class for measurement and monitoring applications. Accordingly, such a kind of harmonic phasor estimator is also expected to be embedded in P-class PMUs. In the IEEE standard, the reference algorithm for P-class PMUs is two cycles long. Although there are no standards for harmonic phasor measurement yet, the IEEE standard framework for fundamental synchrophasor measurement can still be referred to. Thus, the goal of this paper is to develop a two-cycle harmonic phasor estimator for fast harmonic phasor estimation. Also, the estimator should have high accuracy and low complexity. However, there are some challenges to meet these requirements. For example, fault currents could contain decaying dc (ddc) component, which has a detrimental effect on harmonic phasor estimation. Furthermore, when the ddc component is present, it is hard to achieve low complexity and high accuracy simultaneously.

There are many harmonic phasor estimation algorithms in the literature [3], [5], [6], [9]–[17]. However, few of them are well designed for P-class PMUs. The discrete Fourier transform (DFT) is widely used for harmonic phasor estimation because of its simplicity. Unfortunately, it has large errors under frequency deviation, harmonic oscillation, and ddc offset conditions. Window functions and interpolation methods were adopted to immune the effects of frequency deviations [9], [10].

Unlike the DFT that uses a static phasor model, the Taylor–Fourier transform (TFT) describes the dynamic harmonic phasors based on the Taylor signal model [11]. As a result, the designed finite impulse response (FIR) filters have wider passbands and stopbands than the equivalent filters of the DFT. Furthermore, the adaptive TFT can widen the passbands and stopbands of the TFT by a first frequency estimation [12]. In order to adapt the frequency bandwidth variations of different order harmonics, Chen *et al.* [13] proposed a new dynamic harmonic phasor model based on the Shannon sampling theorem, where a parameter can be modified for different order harmonics. When considering the detrimental effects of interharmonics, the compressive sensing of the Taylor–Fourier multifrequency (TFM) model was proposed in [14] to suppress interharmonic interferences. However, when there are many frequency components in a voltage/current signal, it will have high complexity. The fast-TFM devotes to reduce the complexity by simplifying the procedures of seeking frequency components [15].

Other methods, such as the Kalman filter [5], [6], the multiple-resonator-based harmonic phasor estimator [16], and the estimation of signal parameters using rotational

invariance technique (ESPRIT) [17], were also proposed for harmonic phasor estimation.

Although the harmonic phasor estimators mentioned earlier could be applied in various areas, few of them have dealt with the challenges mentioned earlier, especially for improving the accuracy under ddc offset conditions. In [3], the DFT-based harmonic phasor estimator was proposed with the consideration of ddc offsets. However, the errors are still nonnegligible under frequency deviation and harmonic oscillation conditions.

There are also many fundamental synchrophasor estimators considering ddc offsets. In [18] and [19], the ddc component and the fundamental synchrophasor were both described based on the Taylor signal model. The DFT of the ddc component is estimated and then reduced from the DFT of the signal. In [20], a subspace-based fundamental synchrophasor estimator was proposed, which can have high accuracy even in the presence of ddc offset and interharmonics. In [21], the ddc component is modeled by two exponential functions, but the model time constant (TC) selection scheme was not investigated.

In this paper, a new harmonic phasor estimator for P-class PMUs is proposed, which has fast response, high accuracy, and low complexity. The ddc component is described based on several exponential functions. Furthermore, the optimal model TC set for the exponential function-based fitting is searched based on an enumeration method. Regarding harmonic bandwidth variations, the dynamic harmonic phasor is described based on the Shannon sampling theorem [13]. As a result, an FIR filter bank is designed for harmonic phasor estimation.

The proposed estimator can accurately estimate harmonic phasors under ddc offset, frequency deviation, mutual harmonic interference, harmonic oscillation, and frequency ramp conditions. Because the FIR filters are designed offline, the complexity is very low. Also, because the observation window is two cycles long, the harmonic phasor estimator's response times under transient conditions are always no longer than 40 ms. These excellent performances show that the proposed harmonic phasor estimator is capable of being a P-class PMU algorithm. Besides harmonic phasor estimates, harmonic frequency and ROCOF estimates are also provided to make comparisons with the IEEE standard's statements. Because the proposed harmonic phasor estimator is specially used for P-class PMUs, the proposed algorithm is called the P-class harmonic phasor estimator (P-HPE) in the following.

II. HARMONIC PHASOR ESTIMATOR

A. Signal Model

Generally, a power system signal consisting of a ddc component and several harmonic components can be described as

$$
\begin{aligned}
s(t) = {} & \lambda e^{-\frac{t}{\tau}} + \sqrt{2}a_1(t)\cos(2\pi f_0 t + \phi_1(t)) \\
& + \sqrt{2}a_h(t)\cos(2\pi h f_0 t + \phi_h(t)) \\
& + \sum_{l=2, l \neq h}^{L} \sqrt{2}a_l\cos(2\pi l f_0 t + \phi_l)
\end{aligned}
\tag{1}
$$

where λ and τ are the magnitude and TC of the ddc component, respectively; $a_1(t)$ and $\phi_1(t)$ are the oscillating magnitude and phase of the fundamental, respectively; f_0 is

the nominal frequency; $a_h(t)$ and $\phi_h(t)$ are the oscillating magnitude and phase of the hth harmonic, respectively; a_l and ϕ_l are the static magnitude and phase of the lth harmonic, respectively; L is the maximum harmonic order; and Re{·} represents the operator returning the real part of the phasor. Note that although other harmonics can be dynamic like the hth harmonic, we assume that they are static in this paper. $p_1(t) = a_1(t)e^{j\phi_1(t)}$ is defined as the dynamic fundamental synchrophasor. $p_h(t) = a_h(t)e^{j\phi_h(t)}$ is defined as the hth dynamic harmonic phasor, and $p_l = a_l e^{j\phi_l}$ is the lth static harmonic phasor. If the harmonic synchrophasor is defined as a phasor referred to hf_0, then $p_h(t)$ can also be called as the hth harmonic synchrophasor.

B. Dynamic Harmonic Phasor Model

Because the dynamic harmonic phasor can be seen as a band-limited signal, according to the Shannon sampling theorem, it can be reconstructed using the harmonic phasor samples [13], [21], [22]. Accordingly, in a short observation window, $[-T_w/2, T_w/2]$, $p_1(t)$ and $p_h(t)$ can be approximately described only using several samples, which is given by (see [13])

$$
\begin{aligned}
p_d(t) \approx \sum_{k=0}^{K_d} p_{k,d} \frac{\sin[\pi F_d t - \pi(k - \lceil K_d/2 \rceil)]}{\pi F_d t - \pi(k - \lceil K_d/2 \rceil)} \\
(d = 1, h; T_w/2 < \lceil K_d/2 \rceil / F_d)
\end{aligned}
\tag{2}
$$

where F_d ($F_d \neq 0$) is the sampling rate of $p_d(t)$, and $F_d/2$ should be greater than the maximum frequency of the baseband signal $p_d(t)$; $p_{k,d} = p_d[k/F_d]$ is the phasor sample of $p_d(t)$ at the time of $t = k/F_d$; $K_d \in \mathcal{N}$ is the model order; and $\lceil \cdot \rceil$ denotes the ceiling function. Note that K_d can be an odd number. When K_d is odd, the phasor samples in the left side of $p_d[0]$ will be more than the phasor samples in the right side. Note that F_d can be different for different order harmonics to modify the passband and stopband performances of the corresponding filters.

C. DDC Model

In practice, the magnitude and TC of the ddc component are unknown. In this paper, we use the exponential function-based fitting to approximately describe the ddc component [21], which is given by

$$
s_0(t) = \lambda e^{-\frac{t}{\tau}} \approx \sum_{m=0}^{M} \lambda_m e^{-\frac{t}{\tau_m}} \quad (-T_w/2 \leq t \leq T_w/2)
\tag{3}
$$

where λ_m and τ_m are the model magnitude and model TC of the mth exponential function, respectively; and $M+1$ is the number of the exponential function. When building the model, the model TCs are selected first, and then the model magnitudes are estimated through the least square method. Obviously, the model error is associated with the model TCs. The key to high accuracy is to select proper model TCs. In Section III, the scheme for finding the optimal model TC set is proposed.

D. Harmonic Phasor, Frequency, and ROCOF Estimations

It is assumed that the signal (1) is sampled at sampling rate $f_s = N_0 f_0$, where N_0 is the sampling number of a nominal cycle and is assumed as an even number in this paper. Because the two-cycle observation window is particularly considered in this paper, there are $N_w = 2N_0 - 1$ samples in the observation window $[-T_w/2, T_w/2]$. Note that N_w is set at an odd number to make $t_0 = 0$ at the center of the window. The discrete form of (1) can be represented as follows:

$$
\begin{aligned}
s &\approx E A_0 + \frac{\sqrt{2}}{2} \begin{bmatrix} \Phi & \Phi^* \end{bmatrix} \begin{bmatrix} p_k \\ p_k^* \end{bmatrix} \\
&= \frac{\sqrt{2}}{2} \begin{bmatrix} \sqrt{2}E & \Phi & \Phi^* \end{bmatrix} \begin{bmatrix} A_0 \\ p_k \\ p_k^* \end{bmatrix} \\
&= \frac{\sqrt{2}}{2} \Psi P_k
\end{aligned}
\tag{4}
$$

where $s \in \mathcal{R}^{N_w}$ is a column vector containing N_w samples of $s(t)$; $E \in \mathcal{R}^{N_w \times (M+1)}$ is a matrix containing N_w samples of e^{-t/τ_m}, with $m = 0, 1, ..., M$; $A_0 \in \mathcal{R}^{M+1}$ is a column vector containing λ_m, with $m = 0, 1, ..., M$; $\Phi \in \mathcal{C}^{N_w \times [(K_1 + K_h + 2) + (L-2)]}$ is a matrix containing N_w samples of the basis functions $\Phi_{k,d}$ and Φ_l [see (5) and (6)]; $p_k \in \mathcal{C}^{(K_1 + K_h + 2) + (L-2)}$ is a column vector containing $p_{k,d}$ and p_l; and * is the conjugate operator

$$
\begin{aligned}
\Phi_{k,d} &= \frac{\sin[\pi F_d t - \pi (k - \lceil K_d/2 \rceil)]}{\pi F_d t - \pi (k - \lceil K_d/2 \rceil)} e^{j2\pi d f_0 t} \\
&\quad (d = 1, h; k = 0, 1, ..., K_d)
\end{aligned}
\tag{5}
$$

$$
\Phi_l = e^{j2\pi l f_0 t} \quad (l = 2, 3, ..., H; l \neq h).
\tag{6}
$$

Then, we perform the least square method to obtain the estimates of $p_{k,h}$, which is given by

$$
\hat{P}_k = \sqrt{2} (\Psi^H \Psi)^{-1} \Psi^H s
\tag{7}
$$

where ^{H} denotes the Hermitian operator. According to [13] and [21], harmonic phasor derivatives can be obtained by the harmonic phasor sample estimates $\hat{p}_{k,h}$, which is given by

$$
\begin{aligned}
\hat{p}_h^{(q)}(t)|_{t=t_0} &= \frac{d^q}{dt^q} \left[\sum_{k=0}^{K_h} \hat{p}_{k,h} \frac{\sin[\pi F_h t - \pi (k - \lceil K_h/2 \rceil)]}{\pi F_h t - \pi (k - \lceil K_h/2 \rceil)} \right] \Big|_{t=t_0} \\
&= \sum_{k=0}^{K_h} \hat{p}_{k,h} \frac{d^q}{dt^q} \left[\frac{\sin[\pi F_h t - \pi (k - \lceil K_h/2 \rceil)]}{\pi F_h t - \pi (k - \lceil K_h/2 \rceil)} \right] \Big|_{t=t_0} \\
&\quad (q = 0, 1, ..., K_h).
\end{aligned}
\tag{8}
$$

Obviously, the estimated harmonic phasor is the zeroth derivative $\hat{p}_h^{(0)}(t_0)$, and the harmonic frequency can be estimated by [23]

$$
\hat{f}_h = h f_0 + \frac{1}{2\pi} \frac{\text{Im}\{\hat{p}_h^{(1)}(t_0) \hat{p}_h^{(0)*}(t_0)\}}{|\hat{p}_h^{(0)}(t_0)|^2}
\tag{9}
$$

where $\text{Im}\{\cdot\}$ is the operator returning the imaginary part of the phasor. Traditionally, the harmonic ROCOF is also estimated using the phasor derivative estimates. However, the accuracy of such a method is significantly affected by the wideband noise. This paper uses the second-order fitting method to estimate the

harmonic ROCOF [24]. Generally, the instantaneous harmonic frequency can be described as

$$
\begin{aligned}
\hat{f}_h[n] &\approx R_{h,f0} + R_{h,f1} \frac{n}{f_s} + R_{h,f2} \frac{n^2}{2 f_s^2} \\
&\quad (n = -N_0/2 + 1, ..., 0, ..., N_0/2 - 1)
\end{aligned}
\tag{10}
$$

where $R_{h,f0}$, $R_{h,f1}$, and $R_{h,f2}$ are the zeroth-, first-, and second-derivatives of the instantaneous frequency at $t = 0$, respectively. Equation (10) can be rewritten in the following form:

$$
f_h \approx T_f R_{h,f}
\tag{11}
$$

where $f_h \in \mathcal{R}^{N_0-1}$ is a column vector containing $N_0 - 1$ harmonic frequency estimates; $T_f \in \mathcal{R}^{(N_0-1) \times 3}$ is a matrix containing $N_0 - 1$ samples of 1, t, and $\frac{1}{2}t^2$. Then, the derivatives can be estimated by the least square method, which is given by

$$
\hat{R}_{h,f} = (T_f^H T_f)^{-1} T_f^H f_h.
\tag{12}
$$

Accordingly, the estimated first-derivative $\hat{R}_{h,f1}$ is the harmonic ROCOF estimate. In this paper, the harmonic ROCOF estimator's observation window is one cycle long.

Let the dynamic harmonic order h be $2 \sim L$ one by one. Then, the phasor derivatives estimation filters for each order harmonic can be obtained. The values of K_1, K_h, and M are selected as a tradeoff between the filters' passband and stopband performances. In this paper, they are set to 1, 2, and 2, respectively.

III. OPTIMAL MODEL TC SET

Obviously, when the model TC set is different, the estimator's performance on ddc rejection is different. In this section, we use an enumeration method to find the optimal model TC set $\{\tau_0, \tau_1, \tau_2\}$.

Generally, if the model cannot reconstruct the actual ddc component perfectly, a residual signal will be introduced, which can cause spectral leakage effect on harmonic parameter estimation. In this paper, we use the average power of the residual signal to analyze the spectral leakage effect quantitatively. The reason is shown as follows.

According to Parseval's theorem, we have [25]

$$
\sum_{n=-N}^{N} \frac{\{s_0[n] - \hat{s}_0[n]\}^2}{N_w} = \sum_{k=0}^{N} |C_k|^2
\tag{13}
$$

where $N = (N_w - 1)/2$; C_k is the rms value of the Fourier component of the residual signal at frequency $f = k f_s / N_w$; and $\hat{s}_0[n]$ is the reconstructed signal, which can be obtained by

$$
\hat{s}_0[n] = \sum_{m=0}^{2} \hat{\lambda}_m e^{-\frac{n}{\tau_m f_s}}
\tag{14}
$$

where $\hat{\lambda}_m$ $(m = 0, 1, 2)$ is the estimated magnitude of the exponential function, and is obtained by

$$
\hat{A}_0 = (E^H E)^{-1} E^H s_0
\tag{15}
$$

where $s_0 \in \mathcal{R}^{N_w}$ is a column vector containing N_w samples of $s_0(t)$. The right side of (13) denotes the total spectral leakage effect caused by the residual signal, whereas the left side of (13) is the average power $\bar{p}$ of the residual signal. If the actual ddc component is perfectly reconstructed by the ddc model, there will be no model error, and the ddc interference will be completely rejected. In this condition, the average power is accordingly null. With an increase in the impact of spectral leakage effect (i.e., model error), the average power will also increase. Thus, we can use $\bar{p}$ as an index to represent the ddc model error.

Next, we propose an enumeration method to find the optimal model TC set. Generally, the ddc's TC τ is determined by the fault impedance, fault location, and power system topology. It can vary from 0.01 to 0.1 s [26]. In the proposed enumeration method, the three different model TCs are all selected in the set of {0.01, 0.011, 0.012, ..., 0.098, 0.099, 0.1} s. Obviously, there are many possible combinations of the model TC set. For each combination of the model TC set, the upper bound of $\bar{p}$ is obtained after all the possible ddc offsets (i.e., all possible values of τ, which varies from 0.01 to 0.1 s in a step of 0.001 s) are checked. In each check, λ is always set to 1. Also, only the $\bar{p}$ in the first sliding window is used. This is because the ddc has the most significant impact on the first sliding window (find the proof in the Appendix). Finally, we can obtain the optimal model TC set when the upper bound of $\bar{p}$ is the smallest.

If the sampling frequency f_s is set to 6, 8, and 10 kHz, the optimal model TC set is always {0.011, 0.023, 0.072} s. As seen, the optimal TC set is robust to sampling frequency variations. Moreover, two of the three model TCs (i.e., 0.011 and 0.023) are very small. This is because the ddc with a smaller TC could have a more significant impact on harmonic parameter estimation.

IV. COMPLEXITY AND LATENCY

Because the optimal model TC set is obtained offline, the filters for harmonic phasor, frequency, and ROCOF estimations can be designed offline. Accordingly, the main computations of the P-HPE are for the estimation of the zeroth- and first-derivatives of the harmonic phasor, as well as the harmonic ROCOF. Because the harmonics from the second to the Lth order are considered, $(L-1)(4N_w + 1)(N_0 - 1)$ real multiplications and $(L-1)[(4N_w - 3)(N_0 - 1) - 1]$ real additions are needed for per frame. Because harmonics up to the 13th order are particularly considered in China's synchrophasor standard GB/T 26862-2011 [27], we set L at 13 in this paper. When the sampling frequency is 10 kHz ($f_0 = 50$ Hz), the P-HPE mainly needs 3 813 636 real multiplications and 3 804 072 real additions. Such amount of computations are very small for those digital signal processors which can deliver several billion floating-point operations per second (e.g., TMS320C6713BPYP200 provided by Texas Instruments Inc. [28]).

Because the harmonic phasor and frequency are estimated at the center time of the observation window, the reporting latencies of these two parameters are both 19.90 ms ($f_s = 10$ kHz).

Accordingly, the reporting latency of the harmonic ROCOF is 29.70 ms. They are all smaller than the threshold in the IEEE amendment standard (40 ms for reporting rate RR = 50 frames/s) [8].

V. SIMULATION TESTS

The popular TFT can also reject the ddc by modeling it through the Taylor signal model. This section tests and compares the P-HPE's and TFT's performances under different test conditions, including ddc offset, frequency deviation, wideband noise, mutual harmonic interferences, amplitude and phase modulations, frequency ramp, and step change tests. The total vector error (TVE), absolute frequency error (FE), and absolute ROCOF error (RFE) defined in the IEEE standard are used as the evaluation indices. As is well known, the PMUs used in distribution networks could work in more critical conditions than those used in transmission networks. In order to simulate the worst conditions, M class ranges of the test parameters, such as the modulation frequency ranges, are selected for the following tests, whereas P-class thresholds are used for comparisons.

For a fair comparison, the phasor derivative estimation filters of the TFT are designed based on the same scheme of the P-HPE, and the Taylor signal model for the ddc is also truncated to the second order. In addition, the same harmonic ROCOF estimator is used in the TFT. China's standard GB/T 15 945-2008 states that the absolute power system frequency deviation shall be always smaller than 0.5 Hz [29]. Thus, the fundamental frequency bandwidth is set to 1 Hz. Accordingly, $F_h = 1.15\,h$ Hz is used in the P-HPE to obtain good passband and stopband performances around each harmonic frequency (find more information in [13]). As mentioned earlier, harmonics up to the 13th order are particularly considered in this paper. The sampling frequency is set to 10 kHz. The result of each test is obtained after 1000 repeated runs, in which the fundamental and harmonic phases are uniformly distributed random numbers.

A. DDC Offset Tests

As stated in Section I, the ddc can exist in fault currents. P-class PMUs need to obtain accurate harmonic parameter estimates in such a condition. The test signal is shown in the following equation:

$$s(t) = \lambda e^{-\frac{t}{\tau}} + \cos(2\pi f_0 t + \phi_1) + 0.1\cos(2\pi h f_0 t + \phi_h) \quad h = 2, 3, ..., 13 \quad (16)$$

where λ varies from 10% to 100% of the fundamental amplitude in a step of 10%; τ varies from 0.01 to 0.1 s in a step of 0.01 s; f_0 is set to 50 Hz; ϕ_1 and ϕ_h are uniformly distributed random numbers within $(0, 2\pi)$ rad in 1000 runs.

1) Overall Performances: This section shows the performances of the two estimators when all the possible conditions (i.e., all possible values of λ and τ) are considered. In Fig. 1, the maximum TVEs, FEs, and RFEs of the two estimators are shown. As seen, for all orders of harmonics, the P-HPE is always much more accurate than the TFT in harmonic phasor, frequency, and ROCOF estimations. This is because the ddc
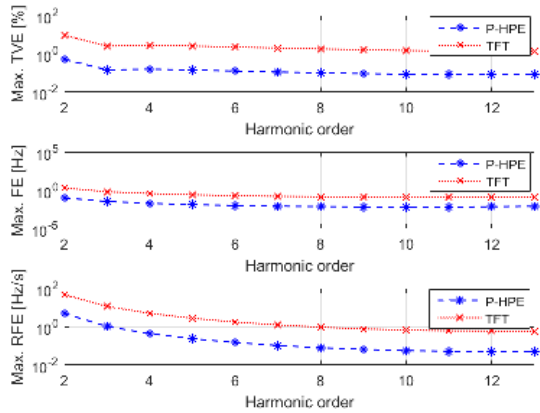
Fig. 1.   Overall maximum TVEs, FEs, and RFEs obtained with the P-HPE and TFT. The *y*-axis of each subplot is shown on a logarithmic scale.
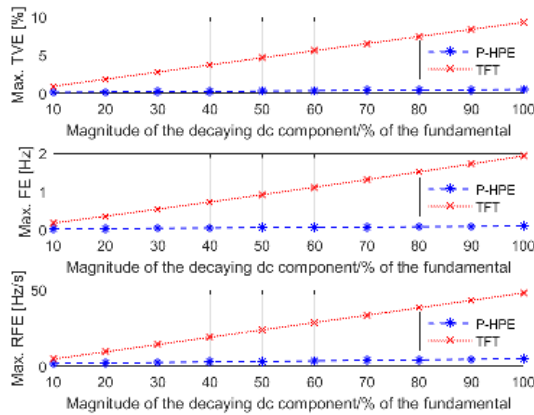

Fig. 2.   Maximum TVEs, FEs, and RFEs with different ddc's magnitudes. The second harmonic parameter estimates are used for illustration.

Fig. 3.   Maximum TVEs, FEs, and RFEs with different TCs. The second harmonic parameter estimates are used for the illustration. The *y*-axis of each subplot is shown on a logarithmic scale.

is perfectly reconstructed by the exponential function-based model. However, the Taylor signal model has large model errors. The application of the optimal model TC set helps to get high accuracy in all the possible ddc offsets. Although a higher order model can help to reduce the model errors of the Taylor signal model, a higher order can also be used in the exponential function-based model. However, using a higher order could make the filters' passband performances worse.

The TFT's overall maximum TVE, FE, and RFE are 9.29%, 1.93 Hz, and 47.92 Hz/s, respectively, whereas the P-HPE's are 0.51%, 0.097 Hz, and 4.93 Hz/s, respectively. In the IEEE standard, the fundamental TVE, FE, and RFE thresholds in modulation conditions are 3%, 0.06 Hz, and 2.3 Hz/s (RR = 50 frames/s), respectively. If such thresholds are also referred to in the ddc offset conditions (they are both dynamic conditions), the P-HPE can fully meet the TVE requirement, whereas its maximum FE and RFE are a bit larger than the thresholds. By contrast, the TFT cannot meet any requirements.

2) Impact of DDC's Magnitude and TC Variations: The results of the P-HPE and TFT with different ddc's magnitudes and TCs are shown in Figs. 2 and 3, respectively. Because the estimates of other harmonics have similar shapes, we take
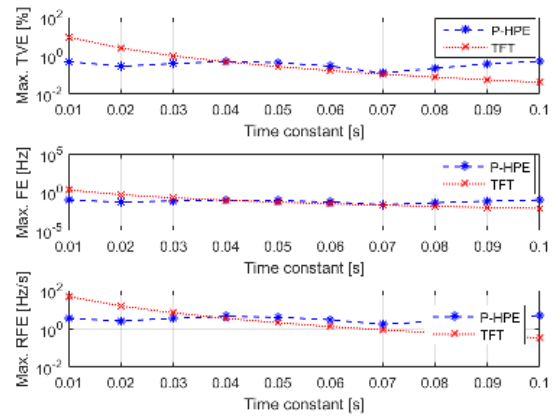
the second harmonic as an example. It is observed that the maximum TVEs, FEs, and RFEs of both estimators are proportional to the ddc's magnitude (see Fig. 2).

In Fig. 3, we can see that with the TC variations, the TFT's TVE, FE, and RFE vary in wide ranges. By contrast, the P-HPE's results are robust to TC variations. This is a key advantage of the P-HPE in harmonic parameter estimation.

In addition, the P-HPE has smaller TVEs, FEs, and RFEs when the TC is about 0.01, 0.02, and 0.07 s. This is because the model TCs used in the P-HPE are 0.011, 0.023, and 0.072 s. When the actual ddc has a TC close to one of the model TCs, it will be significantly rejected by the P-HPE. As a result, the parameter estimation errors will be very small.

B. Frequency Deviation Test With DDC Offset

The test signal is shown in the following equation:

$$s(t) = \begin{cases} \cos(2\pi f t + \phi_1) + 0.1\cos(2\pi h f t + \phi_h) & (t < 0) \\ \lambda e^{-\frac{t}{\tau}} + 1.5\cos(2\pi f t + \phi_1) \\ \quad + 0.15\cos(2\pi h f t + \phi_h) & (t \geq 0) \end{cases}$$
(17)

where f varies from 49.5 to 50.5 Hz in a step of 0.2 Hz; and other parameters are set to the same values in Section V-A. The fault occurred at $t = 0$, and then the ddc component was present in the signal. In Fig. 4, the maximum TVEs, FEs, and RFEs of the 2nd–13th harmonics are shown. When $t < 0$, there is no ddc component, i.e., only the frequency deviation is considered. In such a condition, we can see that the P-HPE is always more accurate than the TFT in harmonic phasor, frequency, and ROCOF estimations, especially for higher-order harmonics (e.g., 8th–13th). This is because the Shannon sampling theorem-based model helps to get better passband and stopband performances than the TFT, especially for higher order harmonics (see [13]). The maximum TVE, FE, and RFE of the P-HPE in such a condition are 0.20%, 0.20 Hz, and 3.11 Hz/s, respectively. In the IEEE standard, their thresholds are accordingly 1%, 0.005 Hz, and 0.4 Hz/s, respectively. Thus, the P-HPE can only meet the TVE requirement.
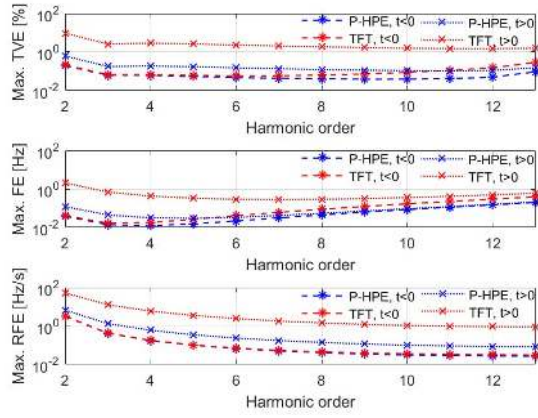
Fig. 4. Maximum TVEs, FEs, and RFEs under frequency deviation and ddc offset condition. $t < 0$ for the signal with the ddc component; and $t \geq 0$ for the signal without the ddc component. The y-axis of each subplot is shown on a logarithmic scale.
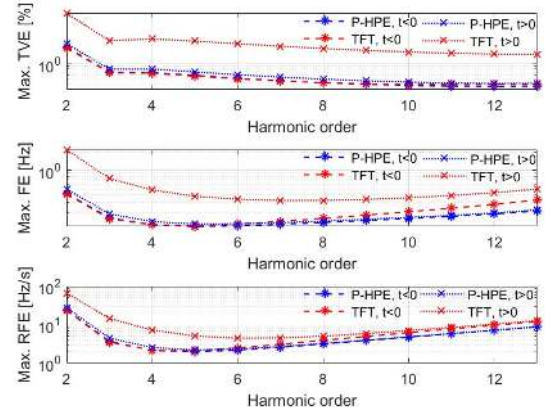

Fig. 5. Maximum TVEs, FEs, and RFEs under harmonic oscillation and ddc offset condition. $t < 0$ for signal with the ddc component; and $t \geq 0$ for signal without the ddc component. The y-axis of each subplot is shown on a logarithmic scale.

When $t \geq 0$, the two estimators' performances are affected by both frequency deviation and ddc offset. In Fig. 4, we can see that P-HPE is much more accurate than the TFT in all the parameters estimation. The overall maximum TVE, FE, and RFE of the P-HPE are 0.62%, 0.21 Hz, and 6.72 Hz/s, respectively. If the thresholds given in Section V-A are also referred to in this condition, the P-HPE can only meet the TVE requirement.

C. Harmonic Oscillation Test With DDC Offset

In this test, the signal in (18) is used, where f_m is the modulation frequency and is set to 5 Hz; other parameters are set to the same values in Section V-A

$$
s(t)
$$
$$
= \begin{cases}
[1 + 0.1\cos(2\pi f_m t)][\cos(2\pi f_0 t + 0.1\cos(2\pi f_m t) + \phi_1) \\
\quad + 0.1\cos(2\pi h f_0 t + 0.1h\cos(2\pi f_m t) + \phi_h)], & (t < 0) \\
1.5[1 + 0.1\cos(2\pi f_m t)][\cos(2\pi f_0 t + 0.1\cos(2\pi f_m t) + \phi_1) \\
\quad + 0.1\cos(2\pi h f_0 t + 0.1h\cos(2\pi f_m t) + \phi_h)] \\
+ \lambda e^{-\frac{t}{\tau}}, & (t \geq 0).
\end{cases}
$$
$$(18)$$

The corresponding results are shown in Fig. 5. When only harmonic oscillation is present, the P-HPE and TFT almost have the same results for lower order harmonics (e.g., 2nd–5th). However, the P-HPE is more accurate than the TFT in higher order harmonics' parameter estimation, especially in harmonic frequency and ROCOF estimations. In such a condition, the overall maximum TVE, FE, and RFE of the P-HPE are 2.20%, 0.42 Hz, and 24.48 Hz/s, respectively. The corresponding thresholds in the IEEE standard are 3%, 0.06 Hz, and 2.3 Hz/s, respectively. Again, only the TVE can meet the requirement.

When the harmonic oscillation and ddc offset are both present, the P-HPE are much more accurate than the TFT in all the parameter estimations. In addition, the overall maximum TVE, FE, and RFE of the P-HPE become 2.58%, 0.49 Hz,

TABLE I

MAXIMUM TVEs, FEs, AND RFEs UNDER MUTUAL HARMONIC INTERFERENCE CONDITION ($t < 0$)

h	TVE [%]		FE [Hz]		RFE [Hz/s]	
	P-HPE	TFT	P-HPE	TFT	P-HPE	TFT
2	0.09	3.60E-9	0.017	5.08E-10	1.43	1.85E-8
3	0.03	9.05E-10	0.005	1.42E-11	0.18	6.83E-10
4	0.03	1.05E-10	0.003	2.76E-12	0.07	6.84E-11
5	0.02	5.20E-10	0.002	1.31E-11	0.03	1.30E-10
6	0.02	2.70E-10	0.001	2.27E-12	0.02	2.91E-10
7	0.02	3.56E-10	0.001	8.41E-12	0.02	1.15E-10
8	0.02	8.56E-11	0.001	2.39E-12	0.01	3.32E-10
9	0.02	1.25E-10	0.001	1.71E-12	0.01	2.71E-11
10	0.02	1.87E-10	0.001	6.25E-13	0.01	1.27E-11
11	0.02	5.88E-10	0.001	9.09E-13	0.01	1.85E-11
12	0.02	1.14E-9	0.001	3.52E-12	0.01	4.04E-11
13	0.03	7.72E-10	0.002	5.08E-12	0.01	3.77E-11

and 27.45 Hz/s, respectively. Also, only the TVE can meet the requirements reported in Section V-A.

D. Mutual Harmonic Interference Test With DDC Offset

In a voltage/current signal, other harmonics can exist besides the harmonic of interest. They may have some impacts on harmonic parameter estimation. In order to simulate this condition, the signal shown in the following equation is used:

$$
s(t) = \begin{cases}
\cos(2\pi f_0 t + \phi_1) \\
\quad + \sum_{h=2}^{13} 0.1\cos(2\pi h f_0 t + \phi_h) & (t < 0) \\
\lambda e^{-\frac{t}{\tau}} + 1.5\cos(2\pi f_0 t + \phi_1) \\
\quad + \sum_{h=2}^{13} 0.15\cos(2\pi h f_0 t + \phi_h) & (t \geq 0)
\end{cases}
$$
$$(19)$$

where ϕ_1, ϕ_h, λ, and τ are set to the same values in Section V-A.

The corresponding results are given in Tables I ($t < 0$) and II ($t \geq 0$). When the ddc component is also present, the P-HPE is much more accurate than the TFT. When there is only mutual harmonic interference, although the P-HPE's TVEs, FEs, and RFEs are generally larger than the TFT, they

TABLE II
MAXIMUM TVEs, FEs, AND RFEs UNDER MUTUAL HARMONIC
INTERFERENCE AND DDC OFFSET CONDITION ($t \geq 0$)

h	TVE [%]		FE [Hz]		RFE [Hz/s]	
	P-HPE	TFT	P-HPE	TFT	P-HPE	TFT
2	0.51	9.29	0.10	1.93	4.93	47.92
3	0.14	2.52	0.03	0.64	1.03	11.42
4	0.16	2.81	0.02	0.38	0.44	5.00
5	0.14	2.55	0.01	0.26	0.24	2.76
6	0.13	2.26	0.01	0.20	0.15	1.75
7	0.11	2.00	0.01	0.16	0.10	1.24
8	0.10	1.79	0.01	0.14	0.08	0.94
9	0.09	1.62	0.01	0.13	0.07	0.77
10	0.09	1.49	0.01	0.12	0.06	0.67
11	0.08	1.38	0.01	0.12	0.05	0.61
12	0.08	1.31	0.01	0.13	0.05	0.59
13	0.09	1.30	0.01	0.14	0.05	0.58

Fig. 7.　Results of the P-HPE and TFT under frequency ramp condition.

Fig. 6.　Results of the P-HPE and TFT considering noise (SNR = 60 dB).

Fig. 8.　Diagram of the experimental test.

are always very small. Note that although TFT's TVEs, FEs, and RFEs are almost 0 in such a simulation test, it will not happen in actual conditions, because the wideband noise will exist. The corresponding TVE, FE, and RFE thresholds in the IEEE standard are 1%, 0.005 Hz, and 0.4 Hz/s, respectively. Thus, most of the results can meet the requirements except the FE and RFE of the second harmonic.

Moreover, the results of the P-HPE are generally the same as the values in Section V-A.1. This evidence indicates that the mutual harmonic interference is significantly rejected by the P-HPE.

E. Wideband Noise Test

In this section, a voltage/current signal in the presence of additive white Gaussian noise is considered for the test, with a signal-to-noise ratio (SNR) equal to 60 dB [see (20)]. The fundamental and harmonic phases (ϕ_1 and ϕ_h) are uniformly distributed random numbers within $(0, 2\pi)$ rad in 1000 repeated runs

$$s(t) = \cos(2\pi f_0 t + \phi_1)$$
$$+ 0.1\cos(2\pi h f_0 t + \phi_h) + \text{noise} \quad (h = 2, ..., 13). \quad (20)$$

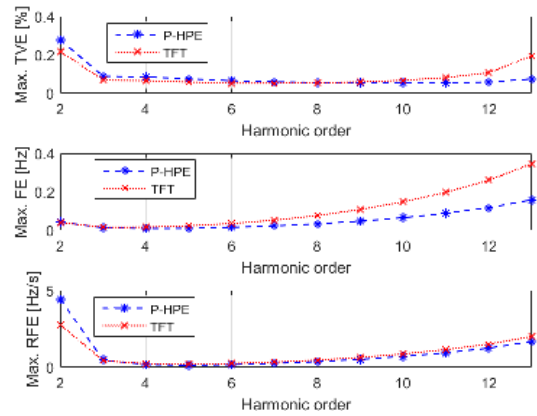The corresponding results are shown in Fig. 6. As shown, the P-HPE has larger TVEs, FEs, and RFEs than the TFT,
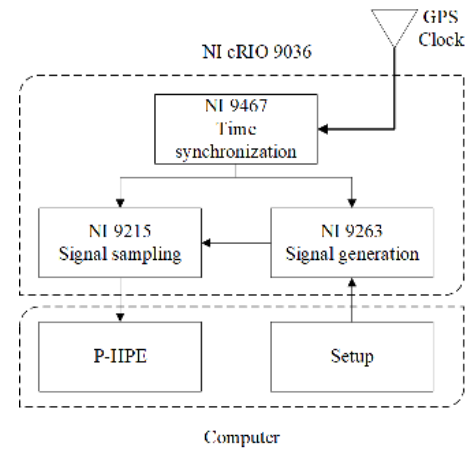
especially for the FEs and RFEs of the lower order harmonics. The reason is that, the exponential function-based ddc model makes the transition band magnitudes of the lower order harmonic filters larger than those of the TFT. The TVE, FE, and RFE thresholds for such condition are 1%, 0.005 Hz, and 0.4 Hz/s, respectively. In Fig. 6, we can see that the P-HPE can only meet TVE requirement.

F. Frequency Ramp Test

This section tests the two estimators' performances under frequency ramp conditions. The test signal is shown in the following equation:

$$s(t) = \cos(2\pi f t + \pi R_1 t^2 + \phi_1)$$
$$+ 0.1\cos(2\pi h f t + \pi h R_1 t^2 + \phi_h) \quad h = 2, ..., 13 \quad (21)$$

where R_1 is the fundamental frequency ramp rate and is set to 1 Hz/s; ϕ_1 and ϕ_h are uniformly distributed random numbers within $(0, 2\pi)$ rad in 1000 repeated runs; and f is set to 49.5 Hz. The fundamental frequency linearly changes from 49.5 to 50.5 Hz. Accordingly, the harmonic frequency linearly changes from 49.5h to 50.5h Hz in a ramp rate of h Hz/s.

The results are shown in Fig. 7. For lower order harmonics (especially for the second harmonic), the P-HPE's TVEs and
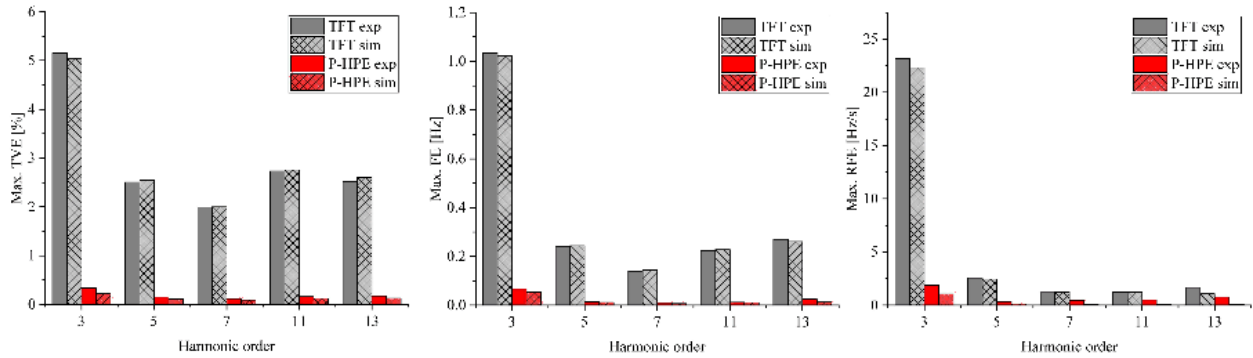
Fig. 9.   Experimental and simulation results returned by the P-HPE and TFT.

TABLE III

MAXIMUM RESPONSE TIMES IN AMPLITUDE STEP CHANGE TEST. THE SYMBOL "−" DENOTES THE RESULTS ARE UNAVAILABLE

h	Phasor [ms]		Frequency [ms]		ROCOF [ms]	
	P-HPE	TFT	P-HPE	TFT	P-HPE	TFT
2	39.70	39.70	-	39.70	-	59.50
3	39.50	39.50	-	39.70	59.30	59.30
4	39.50	39.40	39.70	39.70	59.30	59.30
5	39.50	39.50	39.70	39.70	59.30	59.30
6	39.50	39.50	39.70	39.70	59.30	59.30
7	39.50	39.50	39.70	39.70	59.30	59.30
8	39.50	39.50	39.70	39.70	59.30	59.30
9	39.50	39.50	39.70	39.70	59.30	59.30
10	39.50	39.50	39.70	39.70	59.30	59.30
11	39.50	39.50	39.70	39.70	59.30	59.30
12	39.50	39.50	39.70	39.70	59.30	59.30
13	39.50	39.50	39.70	39.70	59.30	59.30

TABLE IV

MAXIMUM RESPONSE TIMES IN PHASE STEP CHANGE TEST. THE SYMBOL "−" DENOTES THE RESULTS ARE UNAVAILABLE

h	Phasor [ms]		Frequency [ms]		ROCOF [ms]	
	P-HPE	TFT	P-HPE	TFT	P-HPE	TFT
2	39.70	39.70	-	39.70	-	59.50
3	39.50	39.50	-	39.70	59.30	59.20
4	39.50	39.50	39.70	39.70	59.20	59.20
5	39.50	39.50	39.70	39.70	59.20	59.20
6	39.50	39.50	39.70	39.70	59.20	59.10
7	39.50	39.50	39.70	39.70	59.20	59.10
8	39.50	39.50	39.70	39.70	59.20	59.20
9	39.50	39.50	39.70	39.70	59.20	59.20
10	39.50	39.50	39.70	39.70	59.20	59.20
11	39.50	39.50	39.70	39.70	59.20	59.20
12	39.50	39.50	39.70	39.70	59.20	59.20
13	39.50	39.50	39.70	39.70	59.30	59.30

RFEs are larger than the TFT's. This can be seen as the price for using the exponential function-based ddc model. However, for higher order harmonics, the P-HPE is more accurate than the TFT in harmonic phasor, frequency, and ROCOF estimations. This is because the model parameter F_h is modified with an increase in harmonic order, which helps to widen the passband of the filters. In the IEEE standard, the TVE, FE, and RFE thresholds for such a condition are 1%, 0.01 Hz, and 0.4 Hz/s, respectively. Again, the P-HPE can only meet the TVE requirement.

G. Step Change

As for P-class PMUs, fast responses in harmonic phasor, frequency, and ROCOF estimations are required. We use the signal in (20) for such a test. In the amplitude step change test, we assume that the fundamental and the hth harmonic amplitudes change to 90% of the original value at $t = 0.1$ s. Accordingly, in the phase step change test, the phase of each component decreases $\pi/18$ rad at $t = 0.1$ s.

In the IEEE standard, the TVE, FE, and RFE limits for response time calculations are 1%, 0.005 Hz, and 0.4 Hz/s, respectively. If they are also used in this section, the corresponding results are given in Tables III and IV. As shown, the response times of the P-HPE and TFT are generally the same, both under amplitude and step change conditions.

Because the observation windows for harmonic phasor and frequency estimations are both two cycles long, the harmonic phasor and frequency response times are always shorter than 40 ms. Furthermore, because the ROCOF estimator is one cycle long, the ROCOF response times are always shorter than 60 ms. In the IEEE standard, the response time thresholds for fundamental phasor, frequency, and ROCOF estimations are 40, 90, and 120 ms, respectively. If they are also referred for harmonic parameter estimations, the P-HPEs response times are all shorter than the thresholds. Note that because the P-HPEs FEs and RFEs under steady state can be larger than the corresponding limits, the response times are sometimes unavailable (i.e., frequency response times of the second and third harmonics; ROCOF response time of the second harmonic).

VI. EXPERIMENTAL TEST

In order to demonstrate the advantages of the proposed method in actual conditions, an experimental test is carried out. The diagram of the experimental test is reported in Fig. 8. We use an NI 9263 (provided by National Instruments Corporation) to generate a voltage signal [see (22)]. An NI 9215 is used to acquire the signal in a sampling rate of 10 kHz. The two steps of signal generation and signal sampling are synchronized by an NI 9467, which gets accurate time from

the global positioning system (GPS). Finally, the sampled data are delivered to a computer, and the harmonic phasors, frequencies, and ROCOFs are estimated in such a platform

$$s(t) = 4e^{-\frac{t}{0.01}} + 4\cos\left(2\pi f_0 t + \frac{\pi}{5}\right) + 0.2\cos(2\pi \times 3 f_0 \times t)$$
$$+ 0.4\cos\left(2\pi \times 5 f_0 \times t + \frac{\pi}{2}\right) + 0.4\cos(2\pi \times 7 f_0 \times t)$$
$$+ 0.2\cos\left(2\pi \times 11 f_0 \times t + \frac{\pi}{6}\right)$$
$$+ 0.2\cos\left(2\pi \times 13 f_0 \times t + \frac{\pi}{3}\right). \tag{22}$$

The experimental and simulation results are both reported in Fig. 9. Similar to the conclusions in the simulation tests, the maximum TVEs, FEs, and RFEs of the P-HPE in such an experimental test are still much smaller than those of the TFT. These results demonstrate the high performances of the P-HPE in actual conditions. In such an experimental test, the overall maximum TVEs, FEs, and RFEs of the P-HPE are 0.33%, 0.067 Hz, and 1.88 Hz/s, respectively. If the limits given in Section V-A are also referred to in this test, the P-HPE can meet the TVE and RFE requirements.

Generally, the maximum TVEs, FEs, and RFEs of the P-HPE in the experimental test are larger than those in the simulation test. This is due to the errors introduced in the steps of digital-to-analog conversion (NI 9263), analog-to-digital conversion (NI 9215), and time synchronization.

VII. Conclusion

This paper proposed a novel harmonic phasor estimator for P-class PMUs. The exponential functions are used to model the ddc component. Furthermore, the optimal model TC set used in the ddc model is searched based on an enumeration method. The dynamic harmonic phasor is modeled based on the Shannon sampling theorem. Simulation tests show that the proposed method is more accurate than the TFT under ddc offset and frequency deviation conditions. In particular, compared with the TFT, the proposed method is robust to the ddc component's TC variations. The proposed method has short response times in harmonic phasor estimation, which is always no longer 40 ms. Moreover, the proposed method has very low complexity. Such characteristics make the proposed method appropriate to be embedded in a P-class PMU.

Generally, if the IEEE standard is also referred for harmonic phasor estimation, the proposed method can only meet TVE requirements. The FE and RFE limits are too critical for harmonics. An experimental test is implemented to demonstrate the advantages of the P-HPE.

Appendix

Let us assume that the fault occurred at the time of $t = 0$. The discrete form of the ddc component (3) in the first sliding window can be given by

$$s_0[n] = \lambda e^{-\frac{n}{\tau f_s}} \quad n = 0, 1, 2, ..., N_w - 1. \tag{23}$$

However, in the $q + 1$th observation window with initial time of $t = q/f_s$ $(q \in \mathcal{N}^+)$, the discrete ddc component can

be given by

$$s_0[n + q] = \lambda e^{-\frac{n+q}{\tau f_s}}$$
$$= \lambda e^{-\frac{n}{\tau f_s}} e^{-\frac{q}{\tau f_s}}$$
$$= e^{-\frac{q}{\tau f_s}} s_0[n] \quad n = 0, 1, 2, ..., N_w - 1. \tag{24}$$

Thus, if the estimated model TCs in the first sliding window are $\hat{\lambda}_1$, $\hat{\lambda}_2$, and $\hat{\lambda}_3$, they are accordingly $\hat{\lambda}_1 e^{-q/\tau f_s}$, $\hat{\lambda}_2 e^{-q/\tau f_s}$, and $\hat{\lambda}_3 e^{-q/\tau f_s}$ in the $q + 1$th observation window. As a result, the reconstructed $\hat{s}_0[n + q]$ is equal to $e^{-q/\tau f_s} \hat{s}_0[n]$. Then, the aps in the first sliding window and the $q + 1$th window can be given by

$$\bar{p}_1 = \sum_{n=0}^{N_w-1} \frac{\{s_0[n] - \hat{s}_0[n]\}^2}{N_w} \tag{25}$$
$$\bar{p}_{1+q} = \sum_{n=0}^{N_w-1} \frac{\{s_0[n+q] - \hat{s}_0[n+q]\}^2}{N_w}$$
$$= \sum_{n=0}^{N_w-1} \frac{\{e^{-\frac{q}{\tau f_s}} s_0[n] - e^{-\frac{q}{\tau f_s}} \hat{s}_0[n]\}^2}{N_w}$$
$$= e^{-\frac{q}{\tau f_s}} \sum_{n=0}^{N_w-1} \frac{\{s_0[n] - \hat{s}_0[n]\}^2}{N_w}$$
$$= e^{-\frac{q}{\tau f_s}} \bar{p}_1$$
$$\leq \bar{p}_1. \tag{26}$$

Only when the ddc component is perfectly reconstructed (i.e., when τ is equal to one of the TCs in $\{\tau_0, \tau_1, \tau_2\}$), $\bar{p}_{1+q} = \bar{p}_1$. Thus, the ddc component has the most significant impact on the first sliding window.

References

[1] M. Farajollahi, A. Shahsavari, and H. Mohsenian-Rad, "Location identification of high impedance faults using synchronized harmonic phasors," in *Proc. IEEE PES Innov. Smart Grid Technol. Conf. (ISGT)*, Washington, DC, USA, Apr. 2017, pp. 1–5.

[2] Y. Sheng and S. M. Rovnyak, "Decision tree-based methodology for high impedance fault detection," *IEEE Trans. Power Del.*, vol. 19, no. 2, pp. 533–536, Apr. 2004.

[3] Y.-H. Lin, C.-W. Liu, and C.-S. Chen, "A new PMU-based fault detection/location technique for transmission lines with consideration of arcing fault discrimination—Part I: Theory and algorithms," *IEEE Trans. Power Del.*, vol. 19, no. 4, pp. 1587–1593, Oct. 2004.

[4] K. El-Arroudi, G. Joos, I. Kamwa, and D. T. McGillis, "Intelligent-based approach to islanding detection in distributed generation," *IEEE Trans. Power Del.*, vol. 22, no. 2, pp. 828–835, Apr. 2007.

[5] M. Chakir, I. Kamwa, and H. Le Huy, "Extended C37.118.1 PMU algorithms for joint tracking of fundamental and harmonic phasors in stressed power systems and microgrids," *IEEE Trans. Power Del.*, vol. 29, no. 3, pp. 1465–1480, Jun. 2014.

[6] I. Kamwa, L. Geoffroy, S. R. Samantaray, and A. Jain, "Synchrophasors data analytics framework for power grid control and dynamic stability monitoring," *Eng. Technol. Ref.*, pp. 1–22, May 2016. doi: 10.1049/etr.2015.0049.

[7] *IEEE Standard for Synchrophasor Measurements for Power Systems*, IEEE Standard C37.118.1-2011 (Revision of IEEE Standard C37.118-2005), Dec. 2011.

[8] *IEEE Standard for Synchrophasor Measurements for Power Systems—Amendment 1: Modification of Selected Performance Requirements*, IEEE Standard C37.118.1a-2014 (Amendment to IEEE Standard C37.118.1-2011), Apr. 2014.

[9] A. Carta, N. Locci, and C. Muscas, "GPS-based system for the measurement of synchronized harmonic phasors," *IEEE Trans. Instrum. Meas.*, vol. 58, no. 3, pp. 586–593, Mar. 2009.

[10] A. Carta, N. Locci, and C. Muscas, "A PMU for the measurement of synchronized harmonic phasors in three-phase distribution networks," *IEEE Trans. Instrum. Meas.*, vol. 58, no. 10, pp. 3723–3730, Oct. 2009.

[11] M. A. Platas-Garza and J. A. O. de la Serna, "Dynamic harmonic analysis through Taylor–Fourier transform," *IEEE Trans. Instrum. Meas.*, vol. 60, no. 3, pp. 804–813, Mar. 2011.

[12] M. A. Platas-Garza and J. A. O. de la Serna, "Polynomial implementation of the Taylor–Fourier transform for harmonic analysis," *IEEE Trans. Instrum. Meas.*, vol. 63, no. 12, pp. 2846–2854, Dec. 2014.

[13] L. Chen, W. Zhao, Q. Wang, F. Wang, and S. Huang, "Dynamic harmonic synchrophasor estimator based on sinc interpolation functions," *IEEE Trans. Instrum. Meas.*, pp. 1–12, Nov. 2018.

[14] M. Bertocco, G. Frigo, C. Narduzzi, C. Muscas, and P. A. Pegoraro, "Compressive sensing of a Taylor-Fourier Multifrequency model for synchrophasor estimation," *IEEE Trans. Instrum. Meas.*, vol. 64, no. 12, pp. 3274–3283, Dec. 2015.

[15] C. Narduzzi, M. Bertocco, G. Frigo, and G. Giorgi, "Fast-TFM—Multifrequency phasor measurement for distribution networks," *IEEE Trans. Instrum. Meas.*, vol. 67, no. 8, pp. 1825–1835, Aug. 2018.

[16] M. D. Kušljević, J. J. Tomić, and P. D. Poljak, "Maximally flat-frequency-response multiple-resonator-based harmonic analysis," *IEEE Trans. Instrum. Meas.*, vol. 66, no. 12, pp. 3387–3398, Dec. 2017.

[17] S. K. Jain, P. Jain, and S. N. Singh, "A fast harmonic phasor measurement method for smart grid applications," *IEEE Trans. Smart Grid*, vol. 8, no. 1, pp. 493–502, Jan. 2017.

[18] R. K. Mai, L. Fu, Z. Y. Dong, B. Kirby, and Z. Q. Bo, "An adaptive dynamic phasor estimator considering DC offset for PMU applications," *IEEE Trans. Power Del.*, vol. 26, no. 3, pp. 1744–1754, Jul. 2011.

[19] R. K. Mai, L. Fu, Z. Y. Dong, K. P. Wong, Z. Q. Bo, and H. B. Xu, "Dynamic phasor and frequency estimators considering decaying DC components," *IEEE Trans. Power Syst.*, vol. 27, no. 2, pp. 671–681, May 2012.

[20] P. Banerjee and S. C. Srivastava, "An effective dynamic current phasor estimator for synchrophasor measurements," *IEEE Trans. Instrum. Meas.*, vol. 64, no. 3, pp. 625–637, Mar. 2015.

[21] F. Wang, X. Jin, and Z. Wang, "Optimal design of FIR digital filters for dynamic phasor measurement," *Proc. CSEE*, vol. 34, no. 15, pp. 1648–1657, Oct. 2014.

[22] C. E. Shannon, "A mathematical theory of communication," *Bell Syst. Tech. J.*, vol. 27, no. 4, pp. 623–656, Oct. 1948.

[23] J. A. O. de la Serna, "Dynamic phasor estimates for power system oscillations," *IEEE Trans. Instrum. Meas.*, vol. 56, no. 5, pp. 1648–1657, Oct. 2007.

[24] L. Zhan, Y. Liu, and Y. Liu, "A Clarke transformation-based DFT phasor and frequency algorithm for wide frequency range," *IEEE Trans. Smart Grid*, vol. 9, no. 1, pp. 67–77, Jan. 2018.

[25] *Electromagnetic Compatibility (EMC)—Part 4-7: Testing and Measurement Techniques—General Guide on Harmonics and Interharmonics Measurements and Instrumentation, for Power Supply Systems and Equipment Connected Thereto*, document IEC 61000-4-7:2002, Aug. 2002.

[26] G. Benmouyal, "Removal of DC-offset in current waveforms using digital mimic filtering," *IEEE Trans. Power Del.*, vol. 10, no. 2, pp. 621–630, Apr. 1995.

[27] *Test Specification for Synchrophasor Measurement Unit for Power Systems*, document GB/T 26862-2011, Jul. 2011.

[28] (2018). *TI*. [Online]. Available: http://www.ti.com/lit/ds/symlink/tms320c6713b.pdf

[29] *Power Quality-Frequency Deviation for Power System*, document GB/T 15945-2008, Jun. 2008.

Lei Chen received the B.E. degree from North China Electric Power University, Baoding, China, in 2015. He is currently pursuing the Ph.D. degree with Tsinghua University, Beijing, China.

His current research interests include power system wide area monitoring and phasor measurement unit (PMU) algorithms.

Wei Zhao received the Ph.D. degree from the Moscow Energy Institute, Moscow, Russia, in 1991.

He is currently a Professor with the Department of Electrical Engineering, Tsinghua University, Beijing, China. His current research interests include electromagnetic measurement, virtual instrumentation, networked instrumentation system, and cloud-based instrumentation.

Fuping Wang received the Ph.D. degree from Tsinghua University, Beijing, China, in 2002.

He is currently an Associate Research Fellow with the Department of Electrical Engineering, Tsinghua University. His current research interests include circuits and systems and signal processing.

Songling Huang (SM'18) received the Ph.D. degree from Tsinghua University, Beijing, China, in 2001.

He is currently a Professor with the Department of Electrical Engineering, Tsinghua University. His current research interests include electromagnetic measurement and nondestructive evaluation.